

Tailoring Heat Transfer at Silica–Water Interfaces via Hydroxyl and Methyl Surface Groups

Viktor Mandrolko¹, Konstantinos Termentzidis², David Lacroix¹ and Mykola Isaiev¹

¹*Université de Lorraine, CNRS, LEMTA, F 54000 Nancy – France*

²*Univ. Lyon, INSA-Lyon, CETHIL UMR5008, F-69621, Villeurbanne, France*

Corresponding authors: Viktor Mandrolko, email: viktor.mandrolko@univ-lorraine.fr; Mykola Isaiev, email: mykola.isaiev@univ-lorraine.fr

Abstract

Efficient thermal transport across solid-liquid interfaces is essential for optimizing heat dissipation in modern technological applications. This study employs molecular dynamics (MD) simulations to investigate the impact of surface functionalization on heat transfer at the silica/water interface. It has been shown that the surface functionalization changes significantly the wetting characteristics of silica surface: from one hand hydroxyl groups render such surfaces more hydrophilic, while methyl groups more hydrophobic. Here, we reveal that modifying the surface functionalization from methylated to hydroxylated groups results in: (i) up to an approximately eightfold increase in adhesion energy, (ii) a reorientation of interfacial water molecules to align perpendicular to the surface normal, (iii) a reduction in the liquid depletion length near the interface, and (iv) an overall enhancement of interfacial heat conduction. We quantify interfacial thermal resistance through the calculation of the contribution of each functional group to the total heat flux, providing insights into the physical mechanisms governing heat transfer at functionalized interfaces. We demonstrated that manipulation of the concentrations of the functional groups can be used to tailor interfacial thermal transport.

Introduction

Efficient thermal transport across solid-liquid interfaces is indispensable in modern technological applications, where precise control of heat fluxes is crucial for optimizing device performance and ensuring operational reliability. Rather than solely maximizing thermal conductivity, the strategic manipulation of solid-liquid interfaces—facilitated through surface functionalization and structuration—allows for tailored thermal management. This capability is paramount in diverse sectors such as energy storage, electronics cooling, catalysis, and biomedical devices, where efficient and tuneable heat dissipation is imperative for sustained functionality and safety.

Silica, primarily found as silicon dioxide (SiO_2), exists in several crystalline and amorphous forms. Crystalline alpha-quartz is one of the most abundant materials on Earth, constituting 12% of the mass of the Earth's crust¹. Its unique three-dimensional network, where silicon atoms are tetrahedrally coordinated with oxygen atoms, endows silica with remarkable properties, such as high thermal and chemical stability, low thermal conductivity, mechanical strength² and piezoelectric properties³, making it a key component in a wide range of applications^{4–9}. Although crystalline silica exhibits greater thermal resistance at the water interface compared to amorphous silica, it also possesses higher bulk thermal conductivity¹⁰. Thus, its functionalization remains a valuable approach for tuning interfacial thermal resistance in water-interacting systems while preserving robust bulk thermal performance.

Currently, numerous studies are devoted to understanding the silica surface^{11,12}. For instance, the natural passivation of the surface by different radicals, mainly by hydroxyl, was already stated¹³. At the same time, the surface functionalization by the other groups, such as methyl can be performed if a hydrophobic behavior is required. Surface functionalization of silica is a well-established and versatile approach to modify its chemical and physical properties, enabling precise tailoring to meet the needs of various applications in catalysis, sensing, and material science. This process involves the introduction of functional groups such as hydroxyl (-OH), methyl (-CH₃), amino (-NH₂), or carboxyl (-COOH), achieved through methods like grafting, co-condensation, or one-pot synthesis^{14–17}.

The modification of silica surfaces by covalent attachment of functional groups is commonly achieved via reactions between surface silanol groups and organosilanes, such as methyltrimethoxysilane (MTMS), methyltriethoxysilane (MTES), or trimethylchlorosilane (TMCS)¹⁵⁻¹⁷. The sol-gel method remains a popular choice for synthesizing functionalized silica, offering flexibility in tuning its surface chemistry. For instance, co-condensation incorporates methyl-functionalized silanes like MTMS during synthesis, creating uniform distributions of functional groups. Meanwhile, post-synthesis silylation allows precise control of surface coverage and ensures high-performance modifications^{14,15}.

Functionalization with methyl groups (-CH₃) has been particularly effective in enhancing the hydrophobicity of silica surfaces. This process transforms hydrophilic silanol groups (-Si-OH) into hydrophobic Si-CH₃ groups, significantly reducing surface energy and increasing water contact angles to above 140°, indicative of superhydrophobic properties^{16,17}. For example, MTMS and TMCS have been shown to impart remarkable hydrophobicity to silica aerogels and xerogels. The introduction of these groups not only prevents moisture absorption but also enhances the structural integrity of the material by reducing capillary stresses during drying¹⁷.

Various studies have highlighted the advantages of using advanced functionalization methods for modifying silica. One-pot synthesis provides a cost-effective approach with high yields and minimal environmental impact^{15,17}. Furthermore, co-gelation strategies that utilize MTMS or TMCS have demonstrated success in producing monolithic materials with controlled porosity and high thermal stability, making them ideal for applications such as thermal insulation and environmental remediation^{14,16}. Additionally, the use of hybrid methods combining co-condensation and post-synthesis silylation has yielded materials with superior surface properties and improved mechanical strength¹⁷.

By leveraging these versatile methodologies, functionalized silica materials can be precisely designed to meet the requirements of diverse applications, such as optimizing heat transfer, ensuring both scalability and reproducibility. The introduction of -CH₃ groups enhances hydrophobicity, making silica suitable for water-repellent coatings and thermal insulation materials. On the other hand, -OH functionalization increases hydrophilicity, allowing for better interactions in catalysis and adsorption processes^{15,17}.

While contact angle measurements are commonly used to assess wettability, they are not always the most reliable metric, particularly when a surface is highly hydrophilic and the drop spreads into a thin film. In these cases, examining the work of adhesion is more informative, as it directly relates to wettability and provides a clearer picture of surface behaviour. Additionally, for certain substances, measuring the contact angle can be challenging due to factors like drop size dependence, especially when it comes to the nanoscale ¹⁸, which can lead to inconsistencies as described by the Tolman effect.

There is an established connection between surface wettability and thermal characteristics, as these properties are intrinsically linked. Increased wettability (lower contact angle) generally enhances interfacial thermal conductance due to stronger molecular interactions at the solid-liquid boundary. Studies show a linear correlation between interfacial thermal conductance and wettability, indicating that more hydrophilic surfaces enhance heat transfer due to stronger intermolecular interactions ^{19–21}. However, as the contact angle θ decreases, the work of adhesion, which is proportional to $1+\cos(\theta)$ (see Eq. (1)), increases, that can be problematic for certain applications.

$$W_{adh} = \gamma_l (1 + \cos (\theta)) \quad (1)$$

Here γ_l is the liquid-vapor surface tension and θ is the apparent contact angle.

For example, in spray cooling ²², where a liquid is sprayed onto a hot surface for heat removal, excessive adhesion can hinder droplet mobility and evaporation efficiency, reducing cooling performance. In nucleate boiling ²³, increased adhesion can limit bubble detachment frequency, which is critical for maintaining intensive heat transfer. Finally, in capillary-driven cooling ²⁴, excessively high adhesion can lead to capillary flow deterioration in microchannels, diminishing thermal performance.

To optimize thermal transport, it is necessary to design surfaces that balance good thermal conductance with manageable adhesion properties. While a relationship between work of adhesion and thermal transport has been established, it is neither universal nor consistent across different systems, as the slopes differ significantly across different solids and liquids ^{21,25–28}. Moreover, the relationship between work of adhesion and thermal conductance is

not always linear, making work of adhesion alone even less reliable for predictions of thermal transport properties. Several studies have explored this non-linear relationship. For instance, Park and Cahill reported that the thermal conductance of hydrophobic Au/water interfaces varies significantly as the concentration of solutes like D-glucose or NaCl changes, demonstrating that thermal conductance is influenced by factors beyond just the work of adhesion²⁹. Acharya et al. found that while there is an approximately linear dependence of thermal conductance on $\cos(\theta)$, the relationship is not universally applicable across all systems. They indicated that the adhesion energy does not consistently correlate with thermal conductance, implying that other factors influence thermal transport²¹. This variability suggests that while adhesion plays a role in thermal transport, it alone is not sufficient to predict thermal transport properties. Seeking a more comprehensive approach, researchers have explored alternative parameters to better capture the interfacial thermal conductance behavior.

In this context, the concept of depletion length has been introduced as a potentially more universal descriptor, which is the length of the characteristic region near the interface where structural rearrangements of the liquid occur due to surface interactions. Ramos-Alvarado et al. ³⁰ demonstrated that for smooth, non-polar surfaces, the relationship between depletion length and thermal conductance is consistent, yielding identical coefficients across various surface crystallographic planes of silicon and graphene coated silicon surfaces. Similar exponential dependencies with other coefficients were found for different Pd surface crystallographic planes ³¹ and for graphene oxide with different hydroxyl concentration level ³². While for non-conductive surfaces the only mechanism of heat transfer is phonon vibrations ³³, for surfaces functionalized with polar molecules, additional mechanisms influencing thermal transport emerge. These include hybridized interfacial vibrational modes, electron-phonon coupling, and polaritonic interactions, which can significantly alter thermal boundary resistance and energy dissipation processes ³⁴. This variability further complicates predictions, highlighting the need to explore thermal transport properties on more complex, functionalized surfaces. Understanding how surface modifications influence the interplay between wettability, adhesion, and thermal transport is crucial for developing optimized materials for thermal management applications.

Molecular dynamics (MD) simulations have become a powerful tool for exploring surface functionalization of silica. By using computational models, researchers can observe molecular-level interactions and investigate surface properties, such as thermal conductivity and wettability^{11,12,35–37}, in ways that are difficult to replicate experimentally due to practical limitations.

Molecular dynamics (MD) simulations have become a powerful tool for exploring surface functionalization of silica. By using computational models, researchers can observe molecular-level interactions and investigate surface properties, such as thermal conductivity and wettability^{11,12,35–37}, in ways that are difficult to replicate experimentally due to practical limitations. For instance, Deng et al.¹¹ explored the crystal face-dependent wettability of α -quartz, finding the (001) face more hydrophilic than the (100) face due to higher silanol group density, driven by differences in atomic arrangement and surface energy. Similar results were obtained by Abramov et al.³⁶, where they examined how chemical modifications affect quartz surface wettability. They calculated contact angles for the (001) α -quartz surface in both hydroxylated and alkylated states. The hydroxylated surface showed high wettability, while alkylation—introducing methyl groups—shifted it toward hydrophobicity. Bistafa et al.¹² delves into the work of adhesion and interfacial entropy associated with hydroxylated silica surfaces, demonstrating its role in the thermodynamics of wetting. Bonnaud et al.³⁵ investigated water confined in nanoporous silica. They revealed that confinement alters water's structural and dynamical properties. Specifically, they calculated that in pores smaller than 2 nm, water forms ordered, layered structures with reduced mobility, leading to a significant decrease in the self-diffusion coefficient compared to bulk water. This result relates to our study, where we also focused on confined water and its relationship with silica functionalization. Furthermore, recent study by Gonçalves and Termentzidis³⁸ provides valuable insight into the thermal transport properties of functionalized amorphous silica. Their work demonstrates that grafting hydrophobic trimethylsilane onto the silica surface linearly reduces the cosine of the contact angle, disrupts the water hydrogen bond network, and leads to an exponential increase in interfacial thermal resistance. This finding quantitatively establishes a relationship between surface hydrophobicity and thermal conductance—a result that aligns with our own observations.

Building on these insights, we employ MD simulations to investigate how hydroxyl and methyl functional groups modulate both wetting and thermal transport properties by analyzing key interfacial metrics, such as work of adhesion, wetting angle, interfacial thermal resistance, depletion length and the distribution of water molecule angles near the interface. The results contribute to developing a comprehensive framework for engineering advanced silica-based materials tailored for optimal performance in diverse applications.

After the introduction, the article proceeds with a detailed explanation of the simulation methods, including the molecular dynamics framework and force field parameters. The results section then follows, presenting the key findings on wetting behavior, work of adhesion, interfacial thermal resistance, water molecules angle distribution near the surface, along with the geodesic lengths and radial distribution function analysis. Specifically, the wetting angle measurements illustrate how surface functionalization impacts hydrophilicity and hydrophobicity. The work of adhesion calculations provide insight into the energetic interactions at the solid-liquid interface, while the interfacial thermal resistance study quantifies heat transfer efficiency, complemented by an assessment of how the reorientation and spatial distribution of water molecules contribute to the observed thermal behaviors. The article concludes with a discussion of the findings and their implications.

Simulation details

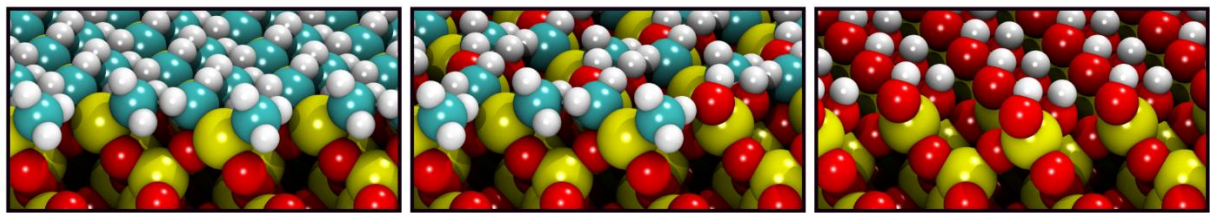
For simulations, classical molecular dynamics was employed, implemented through the LAMMPS package ^{39,40}. Silica was simulated with the modification of alpha-quartz (001) surfaces functionalized with hydroxyl (-OH) and methyl (-CH₃) groups. The density of functionalization groups reached the maximum possible value (9.135 groups/nm²), which results from functionalization of each surface Si atom with either 2 hydroxyl or 2 methyl groups. We used the ClayFF force field ⁴¹, known for its comprehensive treatment of bonded and non-bonded interactions, that was used in other works ^{36,42}. This force field explicitly defines bond lengths and angles for the functional groups, while non-bonded interactions are governed by 12 – 6 Lennard-Jones and Coulomb potentials. The force field parameters were taken from the work of Deng Y ¹¹ The interaction parameters can be found in SM Water was simulated in frames of SPC/E model ⁴³. Since all atoms are charged, each pair of atom species

can interact through Coulombic forces. Regarding the Van der Waals components, the hydrogen atoms in water molecules and hydroxyl groups were excluded from these interactions.

Several silica surface functionalization variants were investigated, ranging from complete hydroxylation to complete methylation. The fully hydroxylated surface corresponds to $N/N_{OH} = 100\%$, where N is the total number of functional groups, and N_{OH} is the number of hydroxyl groups. Intermediate functionalization states were also considered, with decreasing proportions of hydroxyl groups randomly replaced by methyl groups: $N/N_{OH} = 75\%, 50\%, 37.5\%, 25\%, 12.5\%$. The opposite extreme, where all functional groups are methyl, corresponds to $N/N_{OH} = 0\%$. It is worth emphasizing that we considered a fully functionalized surface in each case because the pure silica surface is highly reactive.⁴⁴

Wetting angle measurement

In order to calculate wetting angles, we constructed a system comprising a functionalized silica substrate supporting a droplet in its initial state. By implementing periodic boundary conditions on two sides of the system, it leads to a cylindrical droplet. This choice aimed to simplify the spatial variation of contact angle along the three-phase contact line of a hemispherical droplet and minimize the influence of droplet size effects⁴⁵. The initial configuration of the corresponding system is shown in the lower part of Fig. 1. The bottommost 2 Å of the substrate atoms were restrained to their initial positions using a harmonic potential to mimic the bulk constraints. The system was relaxed using energy minimization. The lower part of the figure shows the initial surface state before relaxation, while the corresponding surface structure after the relaxation and thermostat application can be found in Supplementary Material (Figure S 1).



Methyl

50% Methyl

50% Hydroxyl

Hydroxyl

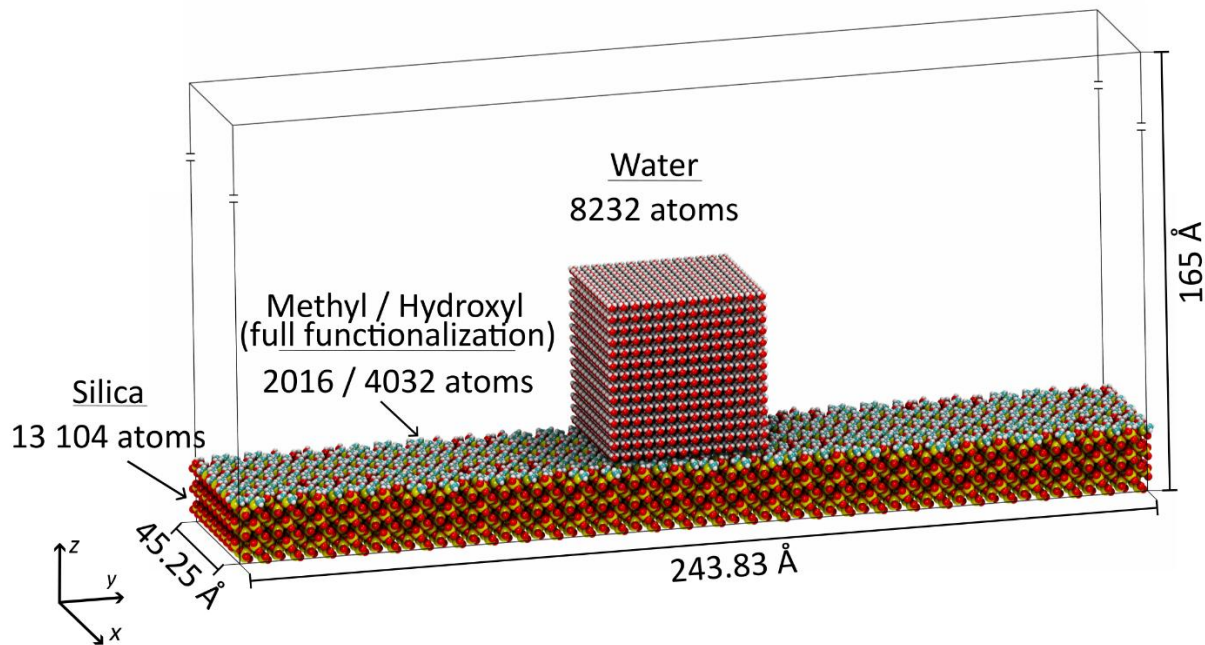


Figure 1. Top: Close-up snapshots of the initial surface states for three functionalization cases—fully methylated, a 1:1 mix of methyl and hydroxyl groups, and fully hydroxylated. Silicon, oxygen, carbon, and hydrogen atoms are represented in yellow, red, turquoise, and white, respectively. Bottom: Initial configuration of a water droplet on a functionalized silica surface.

The dimensions of the simulation box and the quantities of atoms for each species (Si , $-\text{CH}_3$, $-\text{OH}$, and H_2O) are detailed in Table 1.

Table 1. Characteristic lengths of the simulation box and the number of atoms of each species for the system used for the wetting angle measurement.

Simulation box		45.25 Å×243.83 Å×165.0 Å
Silica substrate		45.25 Å×243.83 Å×17.40 Å
Initial configuration of a water droplet		40.3 Å×40.3 Å×40.3 Å
Number of atoms	Silica substrate	13 104
	Water	8 232
	Methyl (-CH ₃) (fully functionalized)	4032
	Hydroxyl (-OH) (fully functionalized)	2016

The simulation was performed in the following order: first, the droplet was heated and thermalized at 300 K for 1.2 ns. Next, it was performed in the NVT ensemble for 10 ns. During this time, 20 density profiles were acquired. The wetting angle was found for each density profile by approximating the droplet surface with a circle. The examples of droplet snapshots and corresponding density profiles are shown in Figure 2.

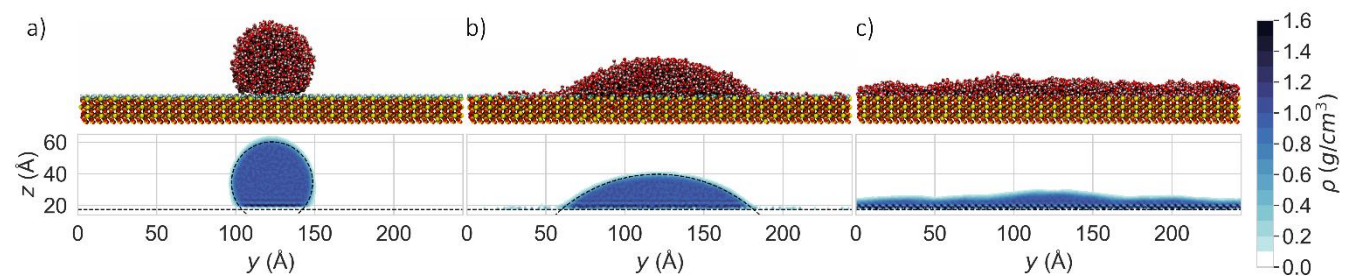


Figure 2. Examples of droplet snapshots and averaged density profiles for: a) the most hydrophobic case (methyl functionalization), b) middle case ($N/N_{OH} = 50\%$) and c) the most hydrophilic case (hydroxyl functionalization)

Next, the contact angle was plotted as a function of time, and the average value was found. Only the wetting angles found in the last 5 ns were considered to ensure the droplet stabilized and reached the optimum contact angle. For each variant of functionalization, three different

simulations were conducted, which differed in the random distribution of functional groups on the surface and random atom velocity generation.

Work of adhesion calculation

The work of adhesion W_{adh} was calculated using the “phantom wall” method⁴⁶. This approach introduces a repulsive potential that selectively interacts with water molecules, allowing controlled liquid separation from the surface. By gradually displacing the wall and measuring the corresponding forces, one can determine the energy required to detach the liquid from the substrate, which directly corresponds to the work of adhesion. This method is widely used due to its conceptual simplicity, robustness, and compatibility with any interatomic potential. We considered a system comprising a solid functionalized silica slab, fully covered by a water layer with a height three times greater than the Lennard-Jones cut-off distance. The characteristic sizes of the system are presented in Figure 3 (in Table 2.)

Table 2. Characteristic lengths of the simulation box and the number of atoms of each species for the system used for the work of adhesion measurement.

Simulation box		35.19 Å×34.83 Å×175.39 Å
Silica substrate		35.19 Å×34.83 Å×22.98 Å
Initial configuration of a water droplet		31.0 Å×31.0 Å×24.8 Å
Number of atoms	Silica substrate	1960
	Water	3267
	Methyl (-CH ₃) (fully functionalized)	224
	Hydroxyl (-OH) (fully functionalized)	448

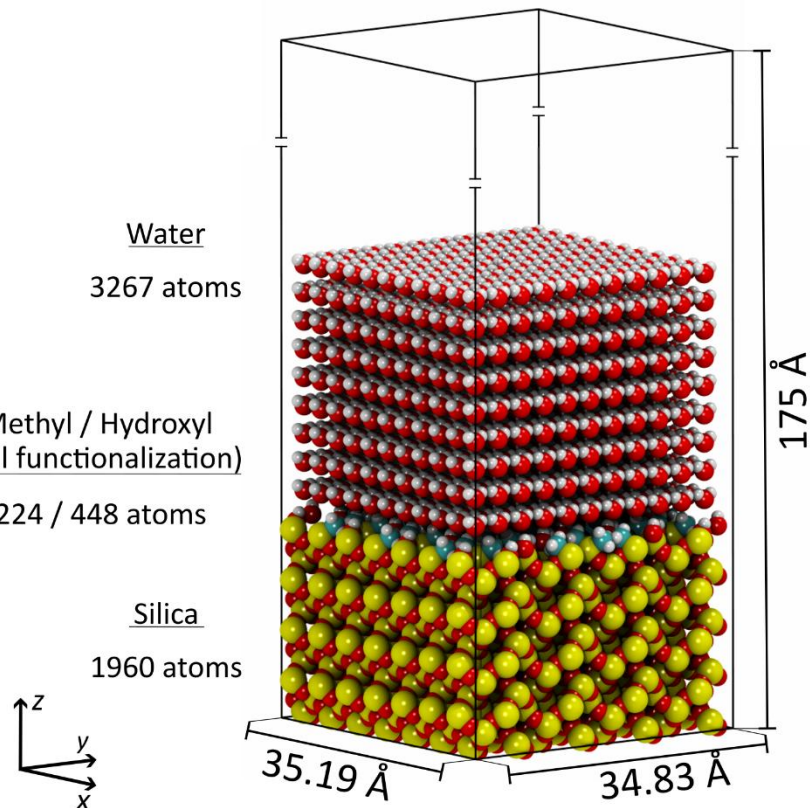


Figure 3. Characteristic lengths of the simulation box and the number of atoms of each species for the system used for the work of adhesion measurement.

The system was first heated and maintained at 300K during 0.5 ns. Then, a repulsive phantom wall perpendicular to the z direction was introduced in a region below the interface to not interact with water molecules (at $z = 18.5 \text{ \AA}$). The wall potential was set to interact exclusively with water molecules (oxygen and hydrogen atoms) and to be transparent for silica. The forces exerted by the wall were calculated based on the 12 — 6 Lennard-Jones potential with parameters $\epsilon = 6.9382 \text{ \AA}$, $\sigma = 3.16 \text{ \AA}$ with cut-off distance 3.546 \AA , rendering the wall repulsive only. The choice of potential is not critical, as long as it ensures a purely repulsive interaction with water molecules and allows the force exerted by the wall to be computed reliably. The wall was then gradually raised to a distance of 9 Å (up to $z = 27.5 \text{ \AA}$) in 70 uniform spatial steps. At each spatial step, the system was first thermalized for 0.1 ns, and then the value of the force exerted by the wall on the water and the system's energy were averaged over 0.5 ns. All calculations were carried out in the NVT ensemble.

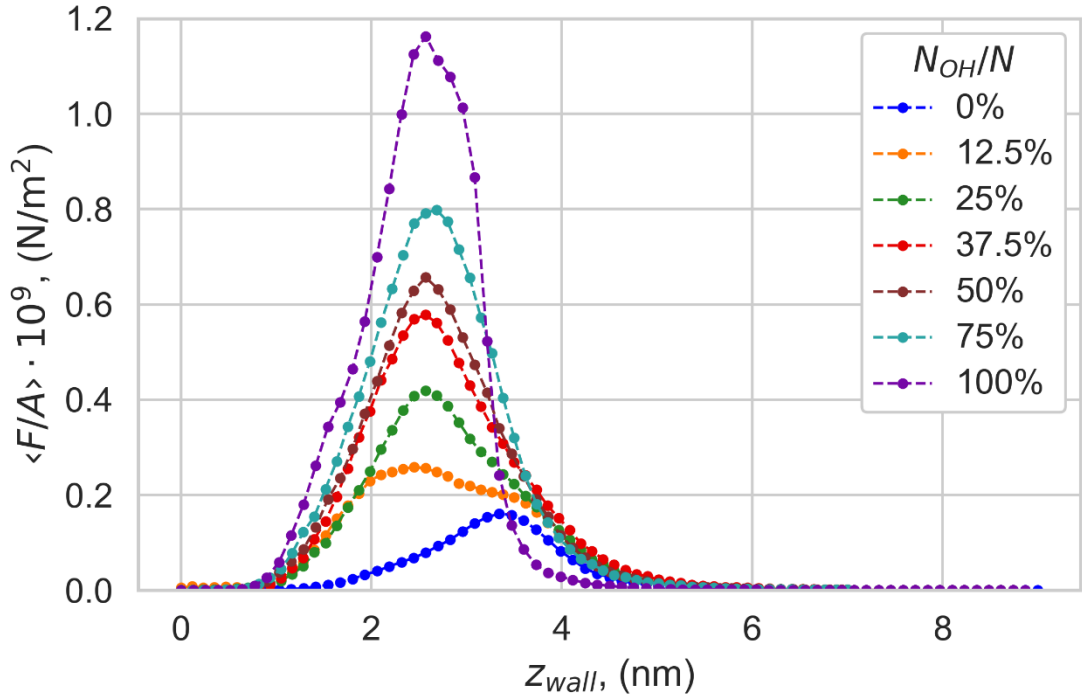


Figure 4. The dependence of force acting on water by the phantom wall on the wall displacement with respect to its initial position.

Fig. 4 depicts the dependencies of the average force per unit area exerted by the phantom wall on water as a function of its displacement from the initial position. Integrating these dependencies provides the work of adhesion:

$$W_{\text{adh}} = \frac{\int_{z_{\text{initial}}}^{z_{\text{final}}} F dz}{A} \quad (2)$$

At the same time, the molecular dynamics method provides us with the capability to directly observe the change in the potential energy of the interaction between the solid and the liquid U , which allows us to measure the interfacial entropy loss per unit area TdS :

$$TdS = U - W_{\text{adh}} \quad (3)$$

Interfacial thermal resistance

The non-equilibrium molecular dynamics method (NEMD) was employed to establish the relation between the functionalization of silica surface and the interfacial thermal transport. Particularly, the heat flux through the interface and interfacial thermal resistance (ITR) were evaluated. The studied system is depicted in the Figure 5. Similar to Klochko et al.²⁰, the simulations were performed with periodic boundary conditions, while sufficient empty space was left in z direction to prevent contact between the top and bottom silica slabs. We considered the following functionalization variants: $N/N_{OH} = 0, 10, 30, 50, 70, 90, 100\%$. The simulation procedure was as follows: first, the system was heated and thermalized at 300 K for 0.35 ns in the NVT ensemble. During relaxation, the liquid volume changed and, after equilibration, reached different values for different functionalization variants. Nevertheless, the water region remained sufficiently large to ensure the presence of a bulk region in the center. We present the volume variation, as well as the change in bulk water density, in Figure S 2. After the thermalization, the most top and bottom layers of atoms with a width of 3 Å were tethered using spring/self in the z direction, and the heat source and sink with a width of 8 Å each were applied in a way to create heat flow through the system. After, the system was held in NVE ensemble for 0.25 ns to reach the equilibrium heat flow, which means that the amount of heat generated by the sours is equal to the amount of heat dissipated by the sink. Subsequent data accumulation was performed over 1 ns during which average amount of energy passing through the system as well as the one-dimensional density profile was obtained.

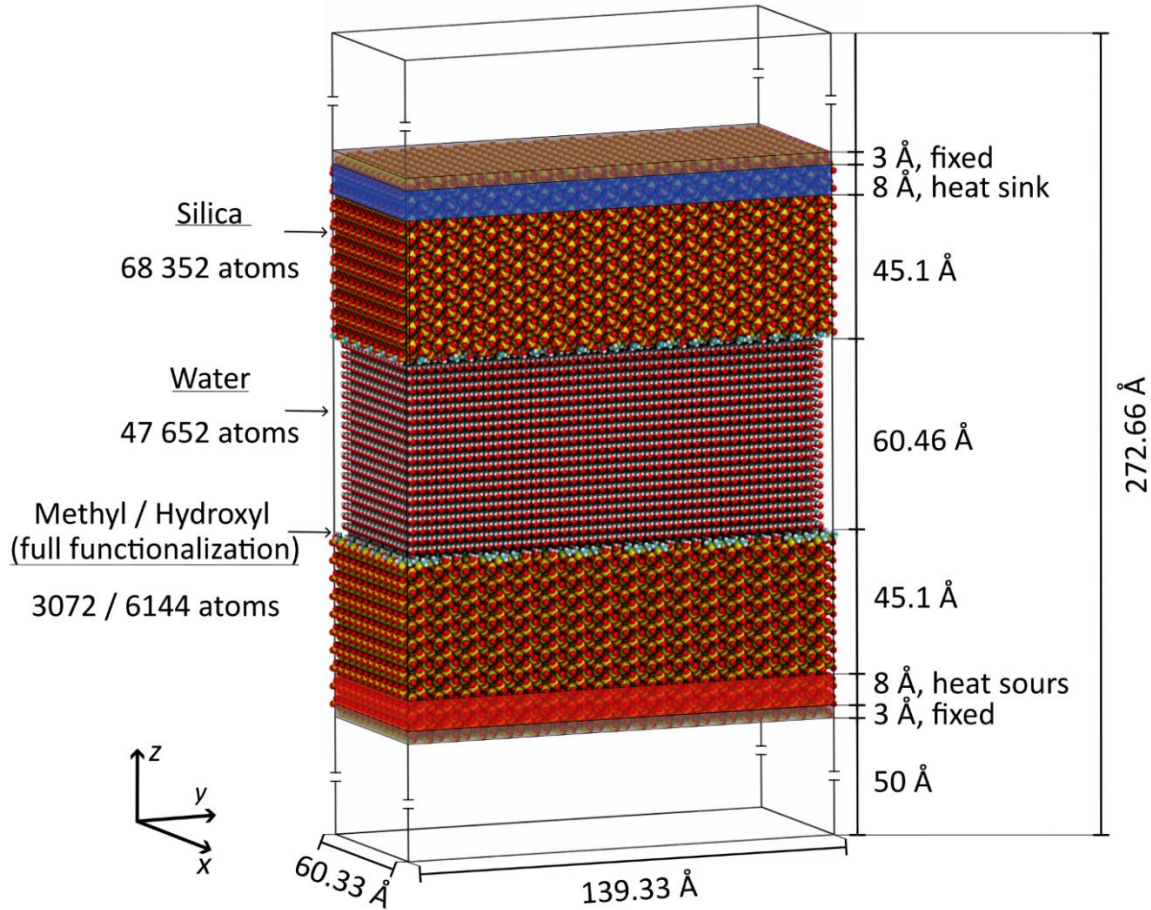


Figure 5. Initial configuration of the system used for the thermal transport measurements.

Given the total amount of energy $\langle E \rangle$ passing through area A in time t , the heat flux was defined as:

$$J = \frac{\langle E \rangle}{A \cdot t} \quad (4)$$

In addition to the heat flux calculation method described above, we also employed an alternative approach that enables the decomposition of heat flux based on the contributions of different atom types, using the following formula:

$$J_{group\ 1 \rightarrow group\ 2} = \sum_{i \in group\ 1} e_i \vec{v}_i + \frac{1}{2} \sum_{i \in group\ 1} e_i \vec{v}_i \sum_{j \in group\ 2} (F_{ij} \cdot \vec{v}_j) \vec{r}_{ij} \quad (5)$$

Here, e_i and \vec{v}_i are the per-atom energy and velocity, respectively; F_{ij} is the force exerted by atom i on atom j ; and \vec{r}_{ij} is the distance vector between them.

Figure S3 depicts J as a function of the surface wettability. To find the temperature jump dT at the solid/liquid interface, one-dimensional density distribution along the z axis was used. The position of the interface was determined based on the definition of the Gibbs dividing surface, from which it follows that ⁴⁷:

$$\int_{-\infty}^{z_{eq}} (\rho_1 - \rho(z)) dz = \int_{z_{eq}}^{\infty} (\rho(z) - \rho_2) dz \quad (6)$$

where z_{eq} is the equilibrium position of interface between solid and liquid phases, $\rho(z)$ – density, and ρ_1, ρ_2 are the bulk densities of both phases. Considering the discrete nature of the data points under analysis, Eq. (6) can be rearranged as:

$$z_{eq} = z_0 + \frac{\langle \rho \rangle - \rho_2}{\rho_1 - \rho_2} \cdot d \quad (7)$$

here $z_0, \langle \rho \rangle, d$ – zero coordinate, average density and width of the considered layer.

Knowing J and dT the interfacial thermal resistance R can be calculated as:

$$R = \frac{dT}{J} \quad (8)$$

Water molecules orientation

Since the thermal transport across the water/solid interface may be connected with the water molecules' orientation⁴⁸, we calculated the probability of orientation of a water molecule relative to the z -axis based on 400 snapshots of the system that was used to calculate the thermal resistance. During the calculations, we considered a near-surface layer of water with a thickness of 10 Å, considering only one water/substrate interface, with the water located above the substrate along the z -axis (see the right part of Figure 12). To analyze the orientation of water molecules relative to the z -axis, we created a histogram of angles from 0 to 180 degrees.

For such a calculation, we considered the number of water molecules in the space limited by the azimuthal angle bins equal to 1°. However, in three-dimensional space, the volume of each angular bin depends on θ due to the spherical coordinate system. Specifically, the volume element is given by:

$$\Delta V \approx \frac{2\pi r^3}{3} \sin \theta \Delta\theta \quad (9)$$

For a fixed radial distance and azimuthal symmetry, the probability density $P(\theta)$ must account for the geometric factor $\sin \theta$. To ensure uniformity, the raw count of molecules in each bin, $N_{H_2O}(\theta)$, was normalized by $\sin \theta$ and the bin width ($\Delta\theta = 1^\circ$):

$$P(\theta) = \frac{N(\theta)}{\sin \theta \cdot \Delta\theta} \quad (10)$$

Results and Discussion

The resulting dependence of wetting angles on time for each functionalization is shown in Figure 6. Variants of 75% and 100% hydroxyl groups functionalization are not shown, because for these cases due to the high hydrophilicity of the surface, the droplet spreads into a film, which aligns with experimental and simulation-based studies at such high hydroxyl concentrations^{37,49}. The red line indicates the wetting angle at which a droplet of a given volume will spread sufficiently so that the distance between it and its periodic image is less than the cut-off distance of the Lennar-Jonnes potential.

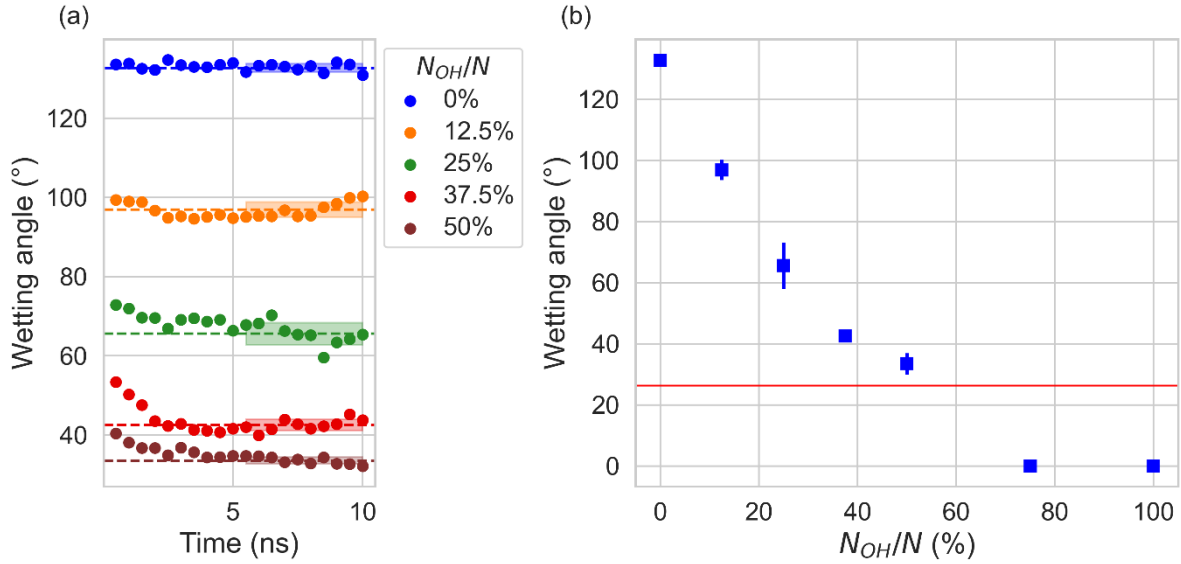


Figure 6. (a) Time dependence of the wetting angle for the considered variants of surface functionalization. Colored bands highlight the data points used for averaging, while dashed lines and band widths indicate the mean wetting angle and its standard deviation (b) Dependence of the wetting angle on the degree of functionalization.

Simulation results for the work of adhesion are presented on Figure 7. Besides, using the Young-Dupré equation, it is possible to calculate the contact angle based on the work of adhesion between liquid and solid:

$$\theta_{YD} = \arccos \left(\frac{W_{adh}}{\gamma_l} - 1 \right) \quad (11)$$

Here γ_l was taken as 63.6 mN/m as was previously reported for the SPC/E water⁵⁰. As shown in Figure 7(b), the contact angles found by the two different methods are in good agreement. Nevertheless, the work of adhesion is a preferable parameter for characterizing the interaction between a solid and a liquid due to its possibility of application to a wider range of interactions.

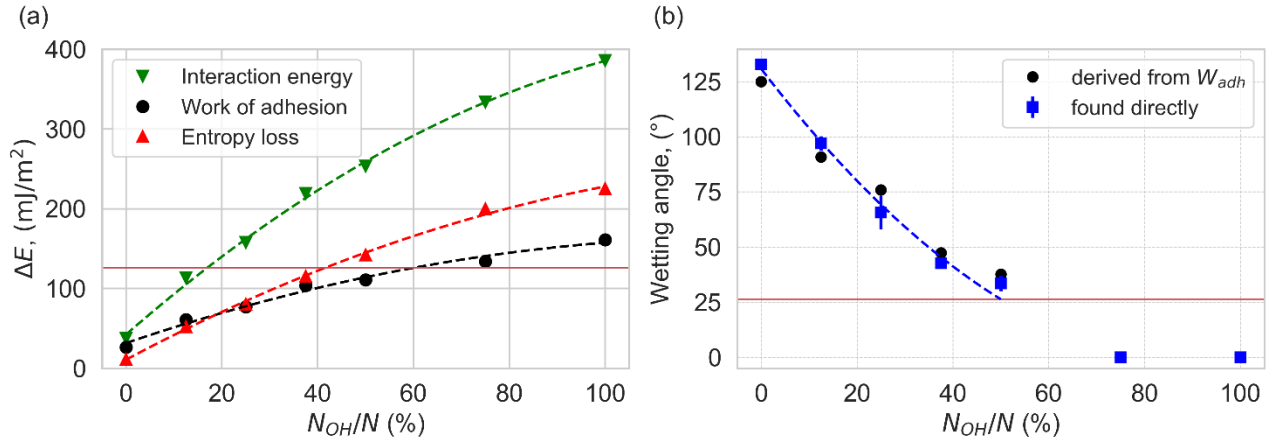


Figure 7. (a) The dependence the work of adhesion, solid-liquid interaction energy and entropy loss per unit area on the functionalization; (b) the comparison of the wetting angles measured directly and derived from the Young-Dupré equation.

The observed increases in three considered with increasing surface functionalization are expected. This behavior can be rationalized by the relation ¹²:

$$u_{SL} = W_{adh} + T\Delta S \quad (12)$$

which links these thermodynamic quantities. Here, u_{SL} represents the average solid-liquid interaction energy per unit area, W_{adh} is the work required to separate the liquid from the solid (i.e., the work of adhesion), and $T\Delta S$ corresponds to the entropic penalty due to the ordering of water molecules at the interface. A higher density of hydroxyl functional groups induces stronger ordering of the interfacial water, leading to more negative interaction energy and requiring greater energy to detach the water layer. This enhanced ordering manifests as a larger entropy loss, as the water near the surface is more structured compared to the bulk.

The heat transfer between the solid and liquid phases is affected by the effective contact between the atoms of the solid and the liquid, which can be characterized by the magnitude of the depletion length³⁰:

$$\delta = \int_0^{\infty} \left[1 - \frac{\rho_s(z)}{\rho_s^b} - \frac{\rho_l(z)}{\rho_l^b} \right] \quad (13)$$

Here $\rho_s(z)$, $\rho_l(z)$ – are the densities of the solid and the liquid phases, ρ_s^b , ρ_l^b – are corresponding densities in bulk region. The depletion length reflects how much the density of the liquid and solid phases deviate from their bulk values at the interface, which directly

impacts the level of interaction between the phases. The variation of δ with surface functionalization is illustrated in Figure 8, where the density distributions for different surface functionalizations are shown: fully methylated, a 1:1 mix of both groups and fully hydroxylated.

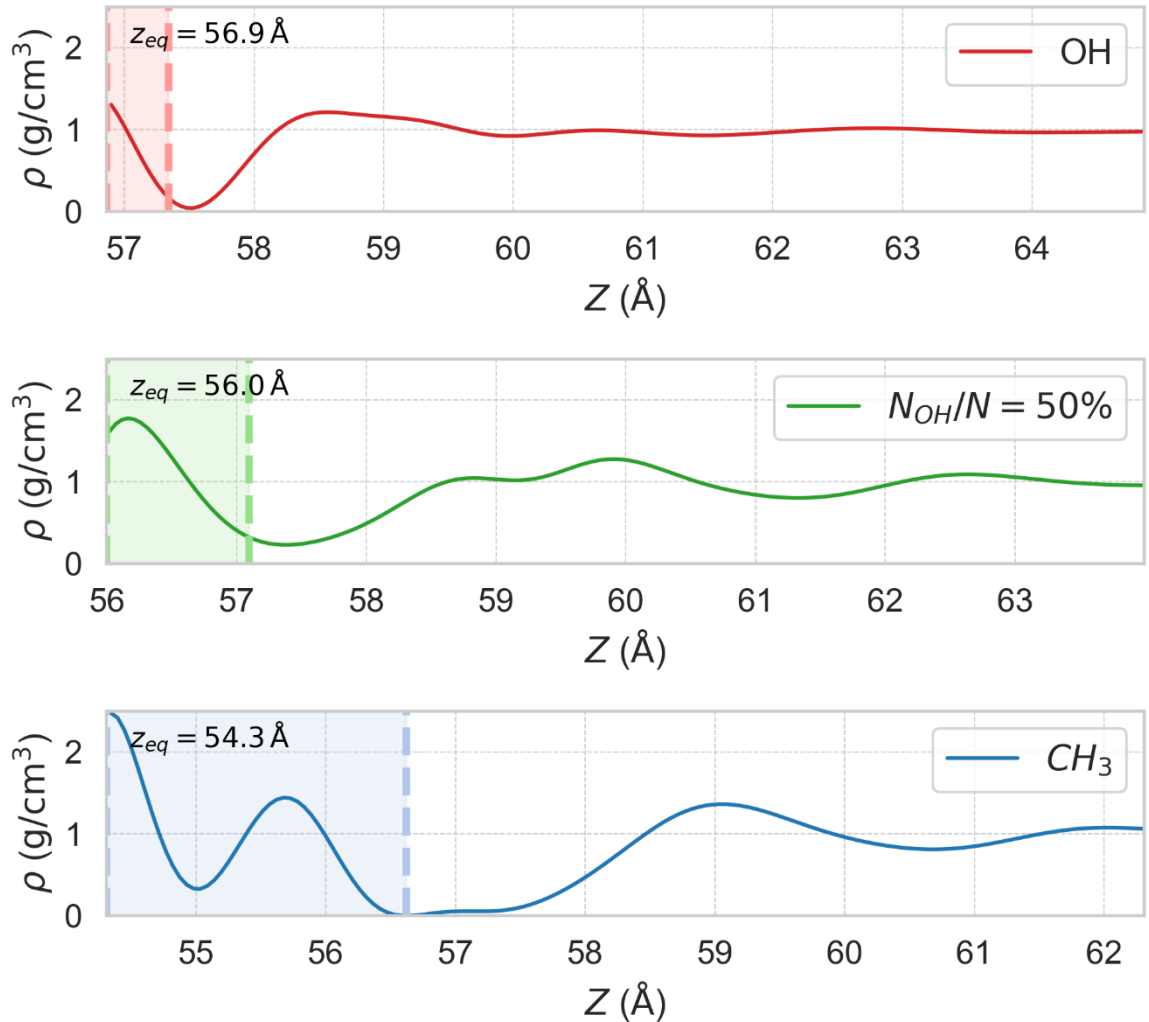


Figure 8. Density distributions of the liquid phase for three representative surface functionalization variants: 100% (OH), 50%, and 0% (CH₃). Each graph starts from the corresponding equimolar dividing interface z_{eq} , with the depletion region highlighted by shading.

These cases are chosen to visually demonstrate how the depletion length varies, and the full range δ dependence is depicted in Figure 9b. The dependence of R on surface

functionalization is illustrated in Figure 9 a., and its relationship with surface wettability is depicted in Fig. S3c.

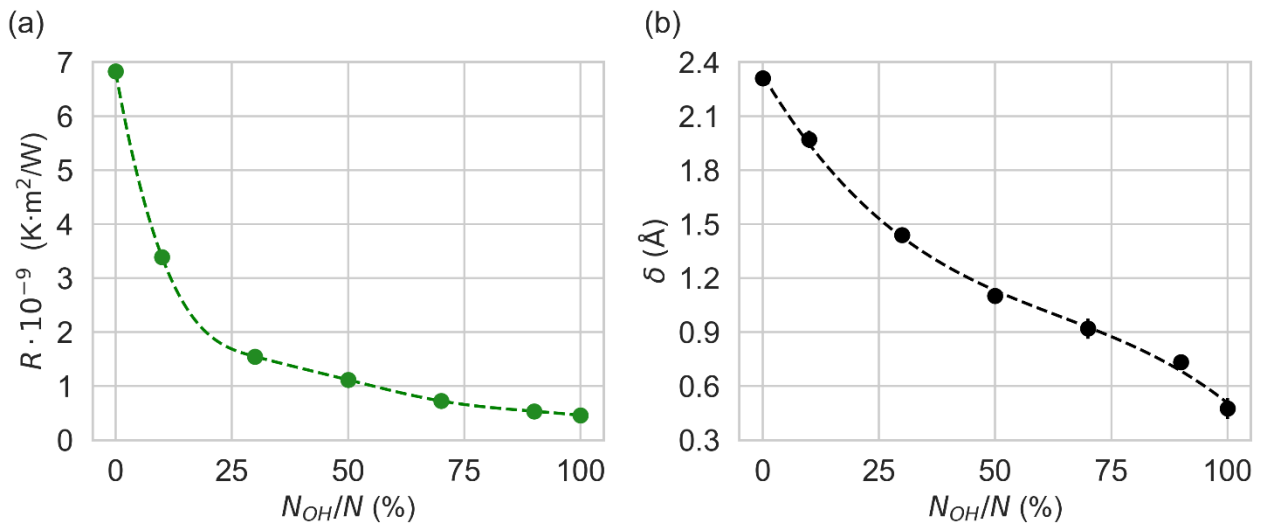


Figure 9. The dependence of R (a) and depletion length (b) on surface functionalization. The dashed lines are for visual guidance.

It can be seen that the thermal resistance decreases with increasing concentration of -OH groups. In addition, the dependence is nonlinear and it is seen that with the addition of 12.5% hydroxyl groups, R decreases by half compared to a fully methylated surface. Similar to the R dependence, depletion length also decreases with increasing hydroxyl concentration. In order to compare the results with the existing ones we also calculated the depletion length for the systems examined in our previous work²⁰, where we analyzed smooth silicon surfaces with varying wettability. Additionally, we compared our results with those of Ramos-Alvarado et al.³⁰, who investigated silicon with different crystal planes and silicon coated with graphene. The results are presented on Figure 10. Here the brown lines are approximating lines of function $Ae^{-b\delta}$ with the parameters: $A = 4302.94$ MW/Km² and $b = 12.99$ nm⁻¹ for silica and $A = 191.48$ MW/Km² and $b = 11.58$ nm⁻¹ for silicon.

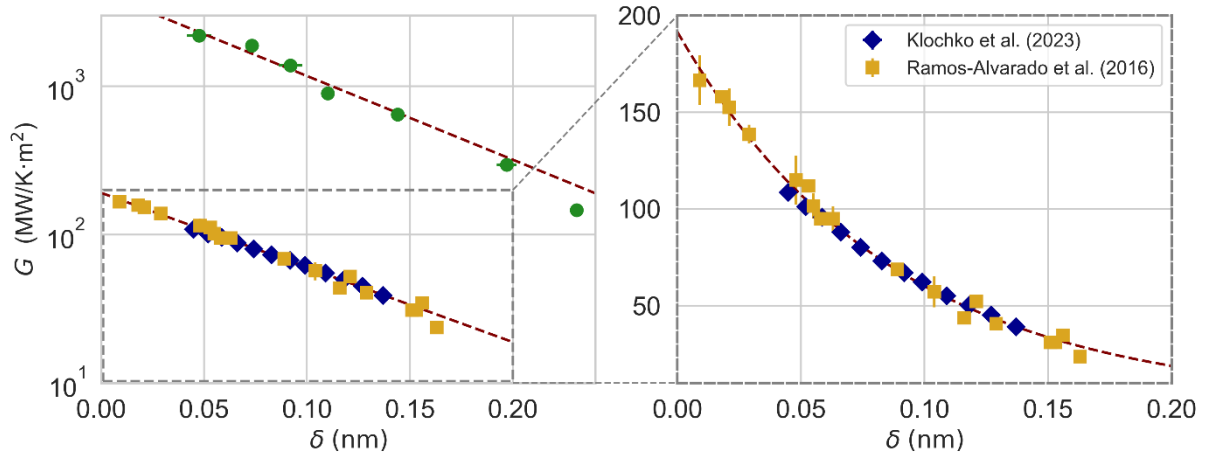


Figure 10. The dependence of interfacial thermal conductance on depletion length for functionalized silica (green circles) in comparison with smooth silicon (100)²⁰ (blue diamonds) and smooth silicon (100)/(111)/silicon coated with graphene³⁰ (yellow squares).

This difference in interfacial thermal conductance for the same depletion length suggests that surfaces with similar wettability may still exhibit significantly different thermal transport properties. To further explore this observation, we compared the dependence of temperature jump, heat flux, and interfacial thermal resistance on the wetting angle for smooth silicon surfaces (from our previous study²⁰) and for the functionalized silica surfaces investigated in the current work. As shown in Figure S 3, for comparable wettability, the silica surfaces exhibit a noticeably smaller temperature jump and a higher interfacial heat flux, resulting in a lower interfacial thermal resistance compared to silicon.

To investigate in more detail how functional groups affect heat transfer, we divided the heat flux into parts depending on which group contributes to it. Figure 11 shows the share of heat flux in percent that is accounted for by bulk atoms, hydroxyl and methyl groups for each considered functionalization variant.

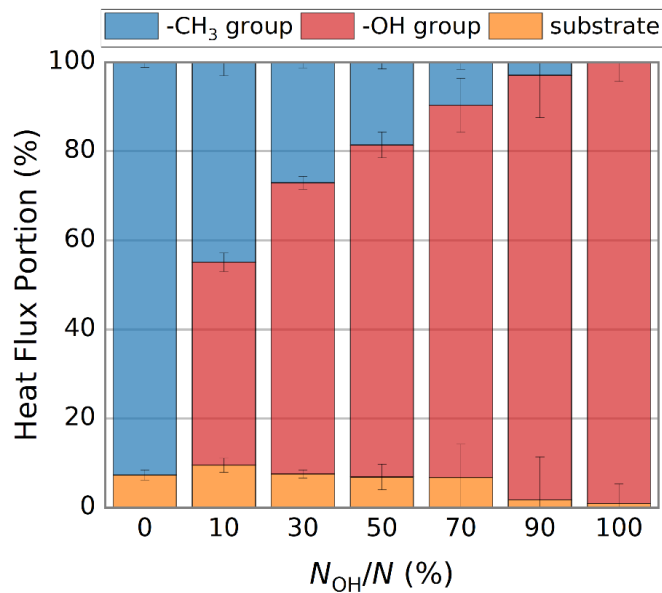


Figure 11. The contribution of the different functionalized groups and the substrate to the total heat flux

The distribution of heat flux components reveals that while only 10% of the silica surface is covered with hydroxyl groups, these groups contribute to 50% of the total heat transfer. This underscores their critical role in heat transfer. The orientation of water molecules relative to the surface can vary depending on the chemical nature of that surface, which in turn can influence its heat transfer properties. This variation is attributed to the formation and organization of hydrogen bond networks ⁴⁸. Water, being a polar molecule, tends to form hydrogen bonds, that depends on how the surface interacts with water. Figure 12 shows the probability distribution of orientations of a water molecule relative to the substrate surface. The hydrophilic (OH-terminated) surface promotes perpendicular molecular alignment, whereas the hydrophobic (CH₃-terminated) surface favors parallel orientations.

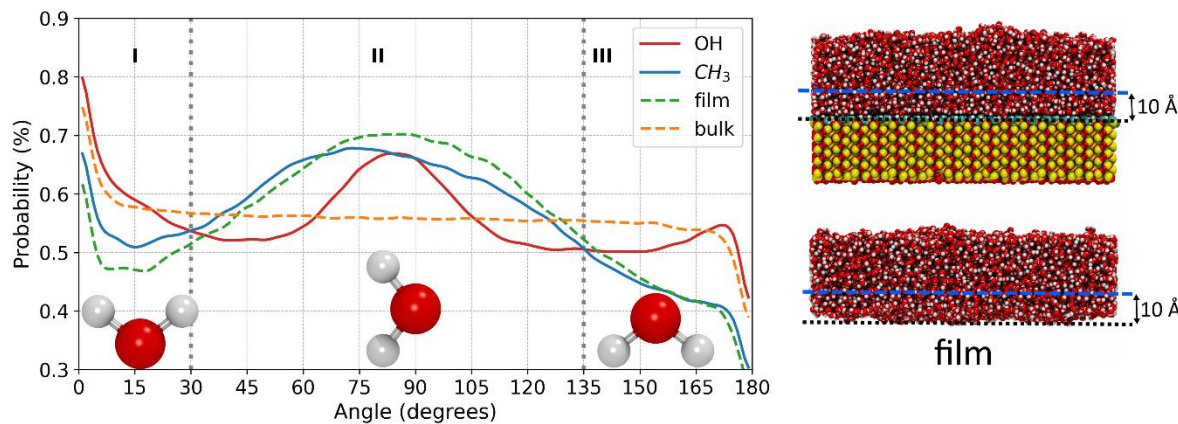


Figure 12. Probability distribution of water molecule orientations relative to the surface normal. The red and blue curves show the distributions for OH- and CH₃-functionalized surfaces, respectively. For comparison, the green and orange dashed curves represent the film (water/vacuum interface) and bulk water. The snapshots on the right show the region where water molecules orientations were taken into account.

The probabilities of water molecule orientations were analyzed in three angular regions: 0–30°, 30–135°, and above 135° denoted as I, II, III. In the case of the hydrophilic (OH-functionalized) surface (red curve) and the hydrophobic (CH₃-functionalized) surface (blue curve), notable differences were observed. On the OH-covered silica surface, water molecules exhibit a pronounced tendency to align along the surface normal, with a normalized probability of 40.30% in the 0°–30° and 135°–180° ranges, compared to 34.72% for the CH₃-covered surface—a relative increase of 16.1%. This aligns with molecular dynamics studies showing that hydroxylated silica surfaces promote ordered water layers with hydrogen-down orientations⁵¹. Conversely, on the CH₃ surface, water molecules are 9.3% more likely to align along the surface plane (30°–135° range) than on the OH surface, reflecting the hydrophobic nature of CH₃ groups. At the water/vacuum interface (film), water molecules show the least tendency to align along the normal, with a probability of lying along the plane higher than both OH and CH₃ surfaces. This planar preference arises from the absence of a solid surface to anchor the molecules, allowing surface tension and dipole interactions to dominate. In contrast, the bulk water exhibits a near-isotropic distribution, serving as a baseline for comparison. These findings confirm that water near the functionalized silica surface is oriented differently depending on the surface chemistry, which should have implications for interfacial phenomena.

It is important to note that the observed asymmetry in the distributions stems from the single-interface configuration of our system, where water is present only above the substrate. This results in an asymmetric distribution of orientations, in contrast to the symmetric curves reported by Wang et al. ⁴⁸ for confined water in nanoporous silicon. The deviation from symmetry is also evident in the film case (see the lower snapshot in Figure 12), where the water/vacuum interface (with vacuum positioned below) yields a similar asymmetric trend. The bulk water distribution is nearly uniform, as expected from the isotropic nature of the system. Additionally, minor anomalies at the angular limits are attributed to the normalization procedure (division by $\sin(\theta)$, see Equation (10)).

Surfaces promoting strong hydrogen bonding, such as hydrophilic (OH-functionalized) surfaces, favor water layers structuration, improving heat transfer. This is because the hydrogen bonds create a pathway along which thermal energy can propagate more easily ^{52–54}. To further investigate the structural differences in the hydrogen bond network near the surface, we analysed the geodesic distances within the network in the same near-surface region of 10 Å thickness as for the molecule's orientation calculations. To establish the existence of a hydrogen bond, the criteria proposed by Ozkanlar and Clark⁵⁵ were used. Surprisingly, the average geodesic length was found to be larger for the hydrophilic surface (24.15) compared to the hydrophobic surface (23.71). This counterintuitive result can be attributed to the interaction between water molecules and the surface. In the hydrophilic case, water molecules tend to form hydrogen bonds with the surface, which can saturate some of their bonding capacity, increasing the geodesic distances. Additionally, the hydrophilic surface exhibits a larger maximum cluster size (2737.6) compared to the hydrophobic surface (2591.7), which can also contribute to longer geodesic paths within the network.

To confirm our understanding of the water structure near the surface, we calculated the radial distribution function $g(r)$ between the surface and water oxygen atoms. Figure 13 shows the $g(r)$ of water O atoms with O in –OH groups and C in –CH₃ groups for two extreme cases.

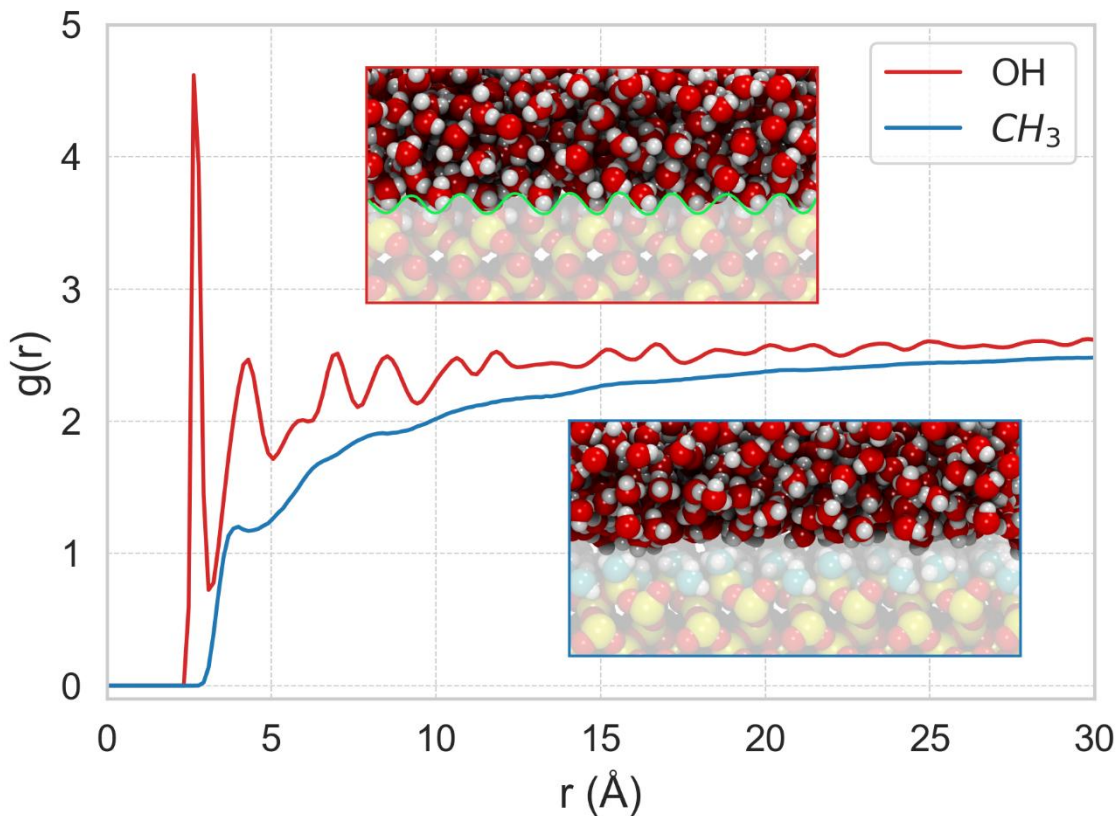


Figure 13. Radial distribution functions $g(r)$ of surface – water oxygen atoms near silica surfaces functionalized with $-\text{OH}$ (red) and $-\text{CH}_3$ (blue) groups, and representative snapshots of water structure at the interface. The green wavy line in the snapshot visually marks the approximate front formed by the water molecules.

In the hydrophilic case, the first $g(r)$ peak appears at 2.64 Å, indicating strong short-range interactions between water molecules and the $-\text{OH}$ terminated surface. Multiple subsequent peaks are also visible, reflecting the formation of a layered, ordered water structure due to hydrogen bonding and surface affinity. In contrast, the hydrophobic surface exhibits a much broader and delayed first peak at 4 Å, with no pronounced secondary peaks, suggesting weak interaction with water and the absence of any significant structuring. The difference is seen on the snapshots, where the water near the $-\text{OH}$ surface shows visible structuring, in contrast to the more diffuse distribution near the $-\text{CH}_3$ surface. This difference arises from the contrasting chemical nature of the functional groups: $-\text{OH}$ groups form hydrogen bonds with water, promoting alignment and layering, while $-\text{CH}_3$ groups are nonpolar and repel water molecules, leading to a more disordered, bulk-like distribution.

Thus, despite the larger geodesic distances within water clusters observed in the hydrophilic case, the structured water layer along with perpendicular water molecule orientation likely enhance heat transfer properties, aligning with our initial hypothesis.

Conclusions

The molecular dynamics simulations performed in this study confirm that surface functionalization dramatically alters the interfacial properties between silica and water, notably affecting wettability, adhesion energy, depletion length, and ITR. The results clearly indicate that tuning the ratio of hydroxyl ($-\text{OH}$) to methyl ($-\text{CH}_3$) groups changes the hydrophilicity of the silica surface and modulates thermal transport across the interface. The following points summarize and explain the observed phenomena:

Hydroxyl groups lead to a denser and more structured arrangement of water molecules at the interface, which increases the local liquid density and reduces the depletion length. This closer molecular packing enhances the physical coupling between the solid and liquid phases, leading to a smaller temperature discontinuity and a more efficient heat flux across the interface. These results are consistent with the idea that a better-packed interfacial region facilitates energy transmission.

Analysis of water molecule orientation shows that water molecules tend to orient more perpendicularly to the surface on hydroxylated surfaces, resulting in improved spatial contact and alignment with the substrate. On the contrary, methylated surfaces promote a more parallel alignment, leading to poorer interfacial interaction. This change in geometric configuration contributes to variations in both the work of adhesion and the observed ITR, confirming the importance of molecular-scale structural effects in thermal transport. This conclusion is further supported by the radial distribution function analysis, which reveals a sharper and closer first peak for hydrophilic surfaces, indicating stronger and more ordered water–substrate interactions compared to the broader, weaker correlations seen near methylated interfaces.

The thermal resistance exhibits a nonlinear behavior with respect to the hydroxyl group concentration. Even a small addition of $-\text{OH}$ groups (e.g., 12.5%) can reduce the ITR by

half compared to a fully methylated surface. This pronounced effect is linked to the decrease in depletion length—a parameter that quantifies the deviation of the liquid density from its bulk value near the interface. The exponential relationship between depletion length and thermal conductance suggests that minor perturbations in the interfacial water structure can lead to significant improvements in heat flow. Thus, the depletion length serves as a useful descriptor for tailoring interfacial thermal properties.

A comparative analysis with earlier work on smooth silicon surfaces and silicon surfaces modified with graphene shows that surfaces having a similar degree of wettability may still differ substantially in their thermal transport characteristics. This indicates that chemical specificity, introduced by different functional groups, plays a decisive role in defining the interfacial heat transfer performance. In the case of functionalized silica, the enhanced contribution of even a small fraction of –OH groups underscores their effectiveness in bridging the energy gap between the solid and liquid phases.

In summary, the study demonstrates that by adjusting the ratio of hydroxyl to methyl groups, one can effectively manipulate both the wetting properties and the heat transfer characteristics of silica surfaces. The enhanced interfacial coupling brought by more favorable water structuring, combined with optimized molecular orientation and reduced depletion length, leads to a lower thermal barrier at the interface. These findings provide a comprehensive framework for designing advanced silica-based materials with tailored thermal properties. A deeper understanding of atomistic thermal transport mechanisms could aid in the design of more efficient heat exchange systems.

Acknowledgment

This research was supported by the ANR project “PROMENADE” No. ANR-23-CE50-0008. Molecular simulations were conducted using HPC resources from GENCI-TGCC, GENCI-IDRIS and GENCI-CINES (eDARI projects No. A0150913052 and A0170913052). We appreciate Dr Samy Merabia from the Institute of Light and Matter (Institut Lumière Matière, Université Claude Bernard Lyon 1, CNRS).

References

- (1) Moore, M. Crystalline Silica: Occurrence and Use. *Indoor and Built Environment* **1999**, *8* (2), 82–88. <https://doi.org/10.1177/1420326X9900800202>.
- (2) Goumans, T. P. M.; Wander, A.; Brown, W. A.; Catlow, C. R. A. Structure and Stability of the (001) α -Quartz Surface. *Physical Chemistry Chemical Physics* **2007**, *9* (17), 2146–2152. <https://doi.org/10.1039/b701176h>.
- (3) Ramus, R. Alpha Quartz. *IEEE Potentials* **1989**, *8* (4), 9–12. <https://doi.org/10.1109/45.43027>.
- (4) Nayl, A. A.; Abd-Elhamid, A. I.; Aly, A. A.; Bräse, S. Recent Progress in the Applications of Silica-Based Nanoparticles. *RSC Adv* **2022**, *12* (22), 13706–13726. <https://doi.org/10.1039/D2RA01587K>.
- (5) Luthfiah, A.; Deawati, Y.; Firdaus, M. L.; Rahayu, I.; Eddy, D. R. Silica from Natural Sources: A Review on the Extraction and Potential Application as a Supporting Photocatalytic Material for Antibacterial Activity. *Science and Technology Indonesia* **2021**, *6* (3), 144–155. <https://doi.org/10.26554/sti.2021.6.3.144-155>.
- (6) Walcarius, A. Analytical Applications of Silica-Modified Electrodes -A Comprehensive Review. *Electroanalysis* **1999**, *10* (18), 1217–1235. [https://doi.org/10.1002/\(SICI\)1521-4109\(199812\)10:18<1217::AID-ELAN1217>3.0.CO;2-X](https://doi.org/10.1002/(SICI)1521-4109(199812)10:18<1217::AID-ELAN1217>3.0.CO;2-X).
- (7) Linhares, T.; Pessoa de Amorim, M. T.; Durães, L. Silica Aerogel Composites with Embedded Fibres: A Review on Their Preparation, Properties and Applications. *J Mater Chem A Mater* **2019**, *7* (40), 22768–22802. <https://doi.org/10.1039/C9TA04811A>.
- (8) Giraldo, L. F.; López, B. L.; Pérez, L.; Urrego, S.; Sierra, L.; Mesa, M. Mesoporous Silica Applications. *Macromol Symp* **2007**, *258* (1), 129–141. <https://doi.org/10.1002/masy.200751215>.
- (9) Zou, H.; Wu, S.; Shen, J. Polymer/Silica Nanocomposites: Preparation, Characterization, Properties, and Applications. *Chemical Reviews*. September 2008, pp 3893–3957. <https://doi.org/10.1021/cr068035q>.
- (10) Zhu, W.; Zheng, G.; Cao, S.; He, H. Thermal Conductivity of Amorphous SiO₂ Thin Film: A Molecular Dynamics Study. *Sci Rep* **2018**, *8* (1). <https://doi.org/10.1038/s41598-018-28925-6>.
- (11) Deng, Y.; Wu, Q.; Li, Z.; Huang, X.; Rao, S.; Liang, Y.; Lu, H. Crystal Face Dependent Wettability of α -Quartz: Elucidation by Time-of-Flight Secondary Ion Mass Spectrometry Techniques Combined with Molecular Dynamics. *J Colloid Interface Sci* **2022**, *607* (Pt 2), 1699–1708. <https://doi.org/10.1016/j.jcis.2021.09.047>.
- (12) Bistafa, C.; Surblys, D.; Kusudo, H.; Yamaguchi, Y. Water on Hydroxylated Silica Surfaces: Work of Adhesion, Interfacial Entropy, and Droplet Wetting. *Journal of Chemical Physics* **2021**, *155* (6). <https://doi.org/10.1063/5.0056718>.

(13) Li, H.; Chen, X.; Shen, D.; Wu, F.; Pleixats, R.; Pan, J. Functionalized Silica Nanoparticles: Classification, Synthetic Approaches and Recent Advances in Adsorption Applications. *Nanoscale*. Royal Society of Chemistry October 14, 2021, pp 15998–16016. <https://doi.org/10.1039/d1nr04048k>.

(14) Bhagat, S. D.; Rao, A. V. Surface Chemical Modification of TEOS Based Silica Aerogels Synthesized by Two Step (Acid–Base) Sol–Gel Process. *Appl Surf Sci* **2006**, *252* (12), 4289–4297. <https://doi.org/10.1016/j.apsusc.2005.07.006>.

(15) Hello, K. M.; Ibrahim, A. A.; Shneine, J. K.; Appaturi, J. N. Simple Method for Functionalization of Silica with Alkyl Silane and Organic Ligands. *S Afr J Chem Eng* **2018**, *25*, 159–168. <https://doi.org/10.1016/j.sajce.2018.05.001>.

(16) Sert Çok, S.; Koç, F.; Dudás, Z.; Gizli, N. The Methyl Functionality of Monolithic Silica Xerogels Synthesized via the Co-Gelation Approach Combined with Surface Silylation. *Gels* **2022**, *9* (1), 33. <https://doi.org/10.3390/gels9010033>.

(17) Çok, S. S.; Gizli, N. Hydrophobic Silica Aerogels Synthesized in Ambient Conditions by Preserving the Pore Structure via Two-Step Silylation. *Ceram Int* **2020**, *46* (17), 27789–27799. <https://doi.org/10.1016/j.ceramint.2020.07.278>.

(18) Burian, S.; Shportun, Y.; Yaroshchuk, A.; Bulavin, L.; Lacroix, D.; Isaiev, M. Size-Dependent Wetting Contact Angles at the Nanoscale Defined by Equimolar Surfaces and Surfaces of Tension. *Sci Rep* **2024**, *14* (1), 31340. <https://doi.org/10.1038/s41598-024-82683-2>.

(19) Tascini, A. S.; Armstrong, J.; Chiavazzo, E.; Fasano, M.; Asinari, P.; Bresme, F. Thermal Transport across Nanoparticle-Fluid Interfaces: The Interplay of Interfacial Curvature and Nanoparticle-Fluid Interactions. *Physical Chemistry Chemical Physics* **2017**, *19* (4), 3244–3253. <https://doi.org/10.1039/c6cp06403e>.

(20) Klochko, L.; Mandrolko, V.; Castanet, G.; Pernot, G.; Lemoine, F.; Termentzidis, K.; Lacroix, D.; Isaiev, M. Molecular Dynamics Simulation of Thermal Transport across a Solid/Liquid Interface Created by a Meniscus. *Physical Chemistry Chemical Physics* **2023**, *25* (4), 3298–3308. <https://doi.org/10.1039/D2CP04601F>.

(21) Acharya, H.; Mozdzierz, N. J.; Kebliński, P.; Garde, S. How Chemistry, Nanoscale Roughness, and the Direction of Heat Flow Affect Thermal Conductance of Solid-Water Interfaces. *Ind Eng Chem Res* **2012**, *51* (4), 1767–1773. <https://doi.org/10.1021/ie2010274>.

(22) Zhang, T.; Mo, Z.; Xu, X.; Liu, X.; Chen, H.; Han, Z.; Yan, Y.; Jin, Y. Advanced Study of Spray Cooling: From Theories to Applications. *Energies*. MDPI December 1, 2022. <https://doi.org/10.3390/en15239219>.

(23) Liang, G.; Mudawar, I. Review of Nanoscale Boiling Enhancement Techniques and Proposed Systematic Testing Strategy to Ensure Cooling Reliability and Repeatability. *Appl Therm Eng* **2021**, *184*, 115982. <https://doi.org/10.1016/j.applthermaleng.2020.115982>.

(24) Zhou, F.; Zhou, J.; Li, X.; Chen, Q.; Huai, X. Enhanced Capillary-Driven Thin Film Boiling on Cost-Effective Gradient Wire Meshes for High-Heat-Flux Applications. *Exp Therm Fluid Sci* **2023**, *149*, 111018. <https://doi.org/10.1016/j.expthermflusci.2023.111018>.

(25) Zhang, T.; Gans-Forrest, A. R.; Lee, E.; Zhang, X.; Qu, C.; Pang, Y.; Sun, F.; Luo, T. Role of Hydrogen Bonds in Thermal Transport across Hard/Soft Material Interfaces. *ACS Appl Mater Interfaces* **2016**, *8* (48), 33326–33334. <https://doi.org/10.1021/acsami.6b12073>.

(26) Huang, D.; Ma, R.; Zhang, T.; Luo, T. Origin of Hydrophilic Surface Functionalization-Induced Thermal Conductance Enhancement across Solid-Water Interfaces. *ACS Appl Mater Interfaces* **2018**, *10* (33), 28159–28165. <https://doi.org/10.1021/acsami.8b03709>.

(27) Harikrishna, H.; Ducker, W. A.; Huxtable, S. T. The Influence of Interface Bonding on Thermal Transport through Solid-Liquid Interfaces. *Appl Phys Lett* **2013**, *102* (25). <https://doi.org/10.1063/1.4812749>.

(28) Pelzl, J.; Kijamnajsuk, P.; Chirtoc, M.; Horny, N.; Eisenmenger-Sittner, C. Correlation Between Thermal Interface Conductance and Mechanical Adhesion Strength in Cu-Coated Glassy Carbon. *Int J Thermophys* **2015**, *36* (9), 2475–2485. <https://doi.org/10.1007/s10765-015-1879-2>.

(29) Park, J.; Cahill, D. G. Plasmonic Sensing of Heat Transport at Solid–Liquid Interfaces. *The Journal of Physical Chemistry C* **2016**, *120* (5), 2814–2821. <https://doi.org/10.1021/acs.jpcc.5b11706>.

(30) Ramos-Alvarado, B.; Kumar, S.; Peterson, G. P. Solid-Liquid Thermal Transport and Its Relationship with Wettability and the Interfacial Liquid Structure. *Journal of Physical Chemistry Letters* **2016**, *7* (17), 3497–3501. <https://doi.org/10.1021/acs.jpclett.6b01605>.

(31) Li, S.; Chen, Y.; Zhao, J.; Wang, C.; Wei, N. Atomic Structure Causing an Obvious Difference in Thermal Conductance at the Pd-H₂O Interface: A Molecular Dynamics Simulation. *Nanoscale* **2020**, *12* (34), 17870–17879. <https://doi.org/10.1039/d0nr04594b>.

(32) Li, S.; Chen, Y.; Li, Z.; Zhao, J.; Wei, N. Role of Hydrogen Bonds in Thermal Conductance at the Graphene Oxide-H₂O Interface. *Int J Heat Mass Transf* **2022**, *183*. <https://doi.org/10.1016/j.ijheatmasstransfer.2021.122125>.

(33) Chen, J.; Xu, X.; Zhou, J.; Li, B. Interfacial Thermal Resistance: Past, Present, and Future. *Rev Mod Phys* **2022**, *94* (1). <https://doi.org/10.1103/RevModPhys.94.025002>.

(34) Giri, A.; Walton, S. G.; Tomko, J.; Bhatt, N.; Johnson, M. J.; Boris, D. R.; Lu, G.; Caldwell, J. D.; Prezhdo, O. V.; Hopkins, P. E. Ultrafast and Nanoscale Energy Transduction Mechanisms and Coupled Thermal Transport across Interfaces. *ACS Nano*. American Chemical Society August 8, 2023, pp 14253–14282. <https://doi.org/10.1021/acsnano.3c02417>.

(35) Bonnaud, P. A.; Coasne, B.; Pellenq, R. J. M. Molecular Simulation of Water Confined in Nanoporous Silica. *Journal of Physics Condensed Matter* **2010**, *22* (28). <https://doi.org/10.1088/0953-8984/22/28/284110>.

(36) Abramov, A.; Keshavarz, A.; Iglauer, S. Wettability of Fully Hydroxylated and Alkylated (001) α -Quartz Surface in Carbon Dioxide Atmosphere. *Journal of Physical Chemistry C* **2019**, *123* (14), 9027–9040. <https://doi.org/10.1021/acs.jpcc.9b00263>.

(37) Emami, F. S.; Puddu, V.; Berry, R. J.; Varshney, V.; Patwardhan, S. V.; Perry, C. C.; Heinz, H. Force Field and a Surface Model Database for Silica to Simulate Interfacial Properties in Atomic Resolution. *Chemistry of Materials* **2014**, *26* (8), 2647–2658. <https://doi.org/10.1021/cm500365c>.

(38) Gonçalves, W.; Termentzidis, K. Interfacial Thermal Resistance between Nano-Confined Water and Functionalized Silica: Molecular Dynamics Simulations. *Int J Heat Mass Transf* **2025**, *242*, 126838. <https://doi.org/10.1016/j.ijheatmasstransfer.2025.126838>.

(39) Plimpton, S. Fast Parallel Algorithms for Short-Range Molecular Dynamics. *J Comput Phys* **1995**, *117* (1), 1–19. <https://doi.org/10.1006/jcph.1995.1039>.

(40) Thompson, A. P.; Aktulga, H. M.; Berger, R.; Bolintineanu, D. S.; Brown, W. M.; Crozier, P. S.; in 't Veld, P. J.; Kohlmeyer, A.; Moore, S. G.; Nguyen, T. D.; Shan, R.; Stevens, M. J.; Tranchida, J.; Trott, C.; Plimpton, S. J. LAMMPS - a Flexible Simulation Tool for Particle-Based Materials Modeling at the Atomic, Meso, and Continuum Scales. *Comput Phys Commun* **2022**, *271*, 108171. <https://doi.org/10.1016/j.cpc.2021.108171>.

(41) Cygan, R. T.; Liang, J. J.; Kalinichev, A. G. Molecular Models of Hydroxide, Oxyhydroxide, and Clay Phases and the Development of a General Force Field. *Journal of Physical Chemistry B* **2004**, *108* (4), 1255–1266. <https://doi.org/10.1021/jp0363287>.

(42) Chen, Y. W.; Chu, I. H.; Wang, Y.; Cheng, H. P. Water Thin Film-Silica Interaction on α -Quartz (0001) Surfaces. *Phys Rev B Condens Matter Mater Phys* **2011**, *84* (15). <https://doi.org/10.1103/PhysRevB.84.155444>.

(43) Berendsen, H. J. C.; Grigera, J. R.; Straatsma, T. P. The Missing Term in Effective Pair Potentials. *J Phys Chem* **1987**, *91* (24), 6269–6271. <https://doi.org/10.1021/j100308a038>.

(44) Rimola, A.; Costa, D.; Sodupe, M.; Lambert, J.-F.; Ugliengo, P. Silica Surface Features and Their Role in the Adsorption of Biomolecules: Computational Modeling and Experiments. *Chem Rev* **2013**, *113* (6), 4216–4313. <https://doi.org/10.1021/cr3003054>.

(45) Burian, S.; Isaiev, M.; Termentzidis, K.; Sysoev, V.; Bulavin, L. Size Dependence of the Surface Tension of a Free Surface of an Isotropic Fluid. *Phys Rev E* **2017**, *95* (6), 062801. <https://doi.org/10.1103/PhysRevE.95.062801>.

(46) Leroy, F.; Dos Santos, D. J. V. A.; Müller-Plathe, F. Interfacial Excess Free Energies of Solid-Liquid Interfaces by Molecular Dynamics Simulation and Thermodynamic Integration. *Macromol Rapid Commun* **2009**, *30* (9–10), 864–870. <https://doi.org/10.1002/marc.200800746>.

(47) Hantal, G.; Jedlovszky, P.; Sega, M. Local Structure of Liquid/Vapour Interfaces Approaching the Critical Point. *Soft Matter* **2023**, *19* (21), 3773–3782. <https://doi.org/10.1039/D3SM00176H>.

(48) Wang, X.; Gonçalves, W.; Lacroix, D.; Isaiev, M.; Gomès, S.; Termentzidis, K. Thermal Conductivity Temperature Dependence of Water Confined in Nanoporous Silicon. *Journal of Physics Condensed Matter* **2022**, *34* (30). <https://doi.org/10.1088/1361-648X/ac664b>.

(49) Lamb A N, R. N.; Furlong, D. D. N. *Controlled Wettability of Quartz Surfaces*; 1982; Vol. 78.

(50) Vega, C.; de Miguel, E. Surface Tension of the Most Popular Models of Water by Using the Test-Area Simulation Method. *J Chem Phys* **2007**, *126* (15). <https://doi.org/10.1063/1.2715577>.

(51) Argyris, D.; Cole, D. R.; Striolo, A. Hydration Structure on Crystalline Silica Substrates. *Langmuir* **2009**, *25* (14), 8025–8035. <https://doi.org/10.1021/la9005136>.

(52) Qu, M.; Huang, G.; Liu, X.; Nie, X.; Qi, C.; Wang, H.; Hu, J.; Fang, H.; Gao, Y.; Liu, W. T.; Francisco, J. S.; Wang, C. Room Temperature Bilayer Water Structures on a Rutile TiO₂(110) Surface: Hydrophobic or Hydrophilic? *Chem Sci* **2022**, *13* (35), 10546–10554. <https://doi.org/10.1039/d2sc02047e>.

(53) Zhou, J.; Lin, S.; Zeng, H.; Liu, J.; Li, B.; Xu, Y.; Zhao, X.; Chen, G. Dynamic Intermolecular Interactions through Hydrogen Bonding of Water Promote Heat Conduction in Hydrogels. *Mater Horiz* **2020**, *7* (11), 2936–2943. <https://doi.org/10.1039/d0mh00735h>.

(54) Xu, Z.; Huang, D.; Luo, T. Molecular-Level Understanding of Efficient Thermal Transport across the Silica-Water Interface. *Journal of Physical Chemistry C* **2021**, *125* (43), 24115–24125. <https://doi.org/10.1017/jfm.2021.1136>.

(55) Ozkanlar, A.; Clark, A. E. ChemNetworks: A Complex Network Analysis Tool for Chemical Systems. *J Comput Chem* **2014**, *35* (6), 495–505. <https://doi.org/10.1002/jcc.23506>.

Supplementary materials

The parameters of the interaction potential were taken directly from Deng Y et al.¹¹ and are duplicated here for convenience:

Table S 1. Bonded interaction potential parameters.

Bond stretching parameters		
Bond type	r_0 (nm)	k_b (kJ mol ⁻¹ nm ⁻²)
O — H	0.100	463905.3
Si — C	0.185	167434.1
C — H	0.109	293009.6
Angle bending parameters		
Angle type	θ_0 (deg)	k_θ (kJ mol ⁻¹ rad ⁻²)
Si — O — H	109.47	251.151
Si — C — H	109.50	418.585
H — C — H	107.80	276.144
C — Si — C	110.0	502.302

Table S 2. Nonbonded interaction potential parameters.

Atomic species	Charge (e ⁻)	σ (nm)	ϵ (kJ mol ⁻¹)
Si (bulk, Si — (OH) ₂)	2.1	0.3302027	7.70406×10^{-6}
Si (Si — (CH ₃) ₂)	1.05	0.3302027	7.70406×10^{-6}
O (bulk)	-1.05	0.3165541	0.650481372
O (Si — (OH) ₂)	-0.95	0.3165541	0.650481372
C (Si — (CH ₃) ₂)	-0.18	0.35	0.276144
H (Si — (OH) ₂)	0.425	0	0
H (Si — (CH ₃) ₂)	0.06	0.25	0.12552

Here the Lorentz-Berthelot combination rule was used to calculate the nonbonded interaction parameters for each pair of atomic species.

To illustrate the effect of relaxation and thermalization, we provide snapshots of the functionalized surfaces from Figure 1, which were used for the wetting angle measurement, after applying the thermostat.

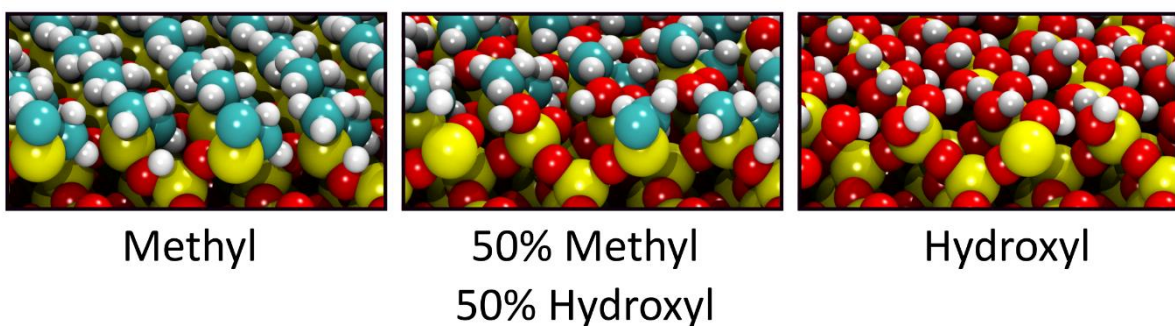


Figure S 1. Snapshots of the functionalized surfaces after relaxation and thermalization.

These structures correspond to those used for the contact angle measurements.

As shown in Figure S 1, the spatial arrangement of surface groups varies depending on their nature. In the fully methylated surface, the relatively large CH_3 groups occupy significant space around each silicon atom, which leads to one of the two groups being oriented toward the interior of the material, while the other points outward. In contrast, on the fully hydroxylated surface, the smaller OH groups tend to bend toward the surface, forming a dense network of hydrogen bonds.

During ITR measurements, we monitored changes in the liquid volume during equilibration to assess the effect of surface functionalization on the water domain. The liquid domain was defined as the region between two equimolar surfaces, calculated using Equation (7). As shown in Figure S 2, the total volume of the water phase decreases with increasing surface density of hydroxyl groups. This trend is expected, as stronger interactions between the polar OH groups and water molecules lead to a more compact and structured interfacial layer, resulting in an overall reduction of the system's liquid volume.

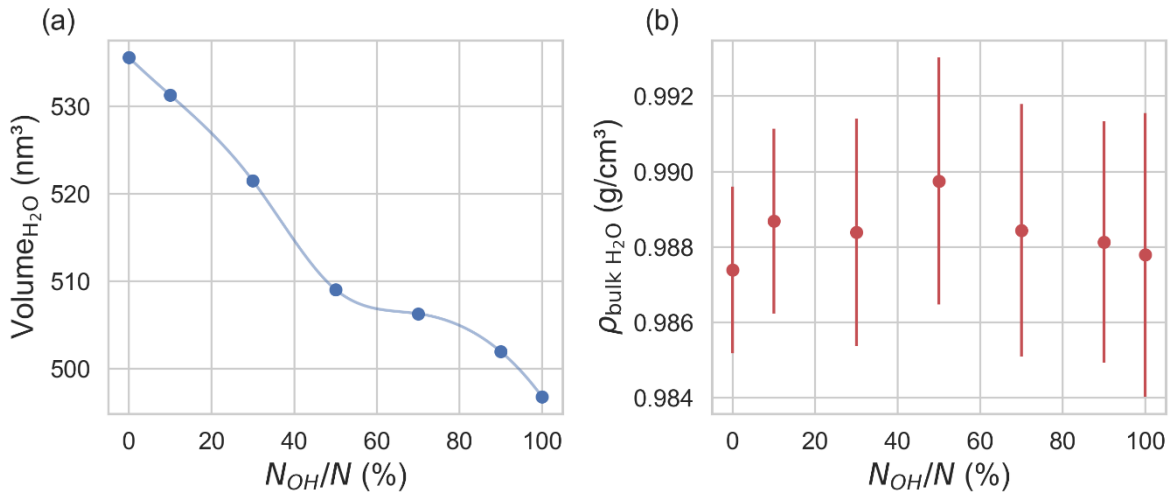


Figure S 2. Dependence on the degree of surface functionalization of (a) the volume of the liquid phase and (b) the density of bulk water. The blue line serves as a visual guide for the eye. The bulk region was defined as a 30 Å thick slab located at the center of the liquid domain. Error bars represent the standard deviation of the average density.

Despite this volume reduction, the central region of the water domain remained large enough to preserve bulk-like behavior. The density of bulk water, measured in a 30 Å thick slab at the center of the domain, remained nearly constant across all functionalization variants, with deviations falling within the margin of statistical uncertainty. This confirms that the presence of a stable bulk region was maintained throughout the simulations.

As seen in Figure S 3, the correlation between heat flux, temperature jump, and thermal resistance with the wetting angle demonstrates that the silica surface exhibits a lower temperature jump and higher heat flux compared to smooth silicon. This results in a noticeable difference in thermal resistance between the two surfaces, with the difference reaching nearly one order of magnitude for certain contact angles.

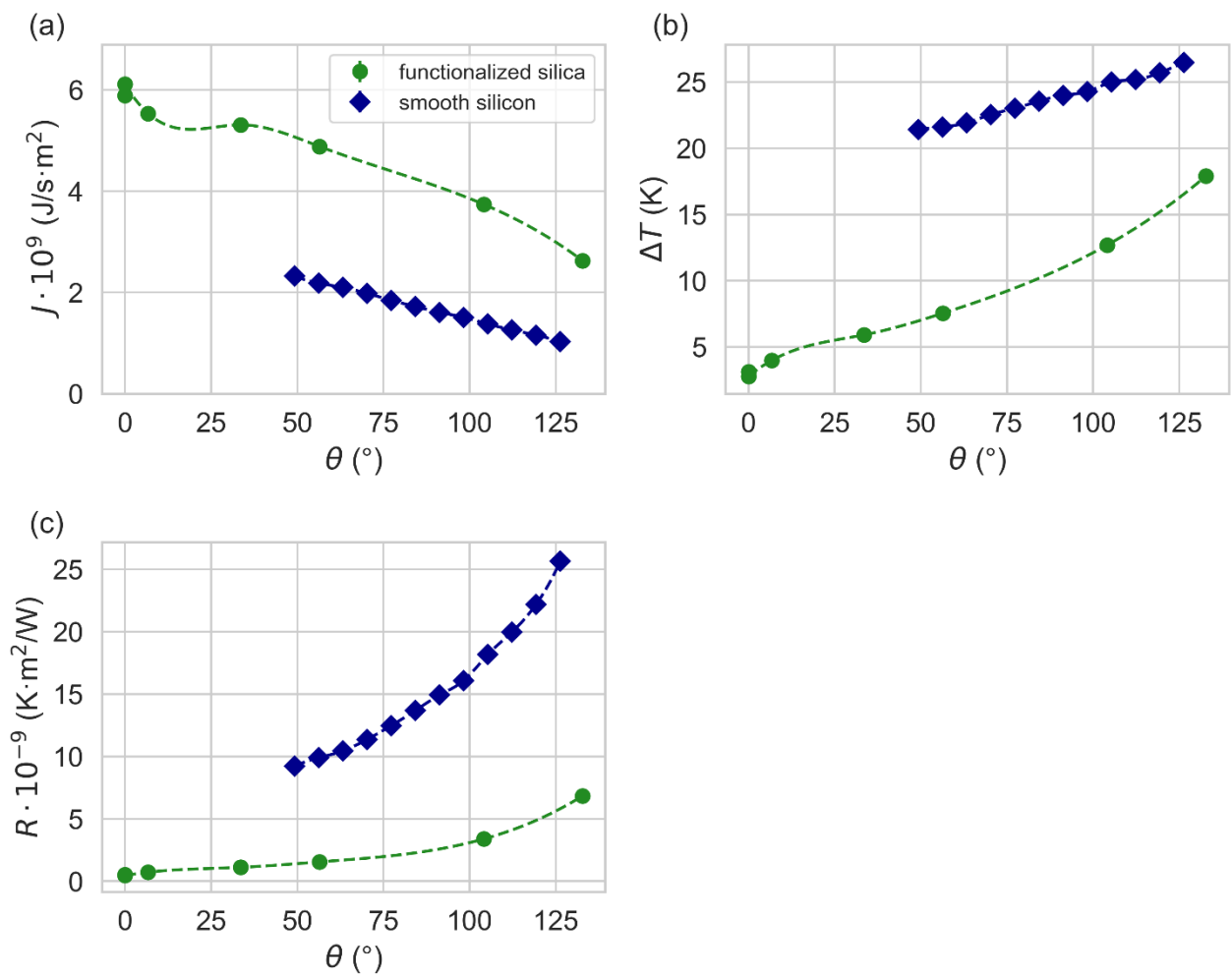


Figure S 3. Correlation of a) heat flux, b) temperature jump and c) thermal resistance with wetting angle for systems with a smooth silicon surface (blue diamonds) and functionalized silica (green circles)